Size and Morphology Adjustment of PVP-Stabilized Silver and Gold Nanocrystals Synthesized by Hydrodynamic Assisted Self-Assembly

ARTICLE *in* THE JOURNAL OF PHYSICAL CHEMISTRY C · MAY 2009

Impact Factor: 4.77 · DOI: 10.1021/jp810668x

6 AUTHORS, INCLUDING:

Licheng Liu
Institute of Chemical and Engineering Scie…
21 PUBLICATIONS **249** CITATIONS

SEE PROFILE

Size and Morphology Adjustment of PVP-Stabilized Silver and Gold Nanocrystals Synthesized by Hydrodynamic Assisted Self-Assembly

Licheng Liu, Ting Wei, Xiao Guan, Xuehong Zi, Hong He,* and Hongxing Dai

Department of Chemistry and Chemical Engineering, College of Environmental and Energy Engineering, Beijing University of Technology, Beijing 100124, China

Received: December 4, 2008; Revised Manuscript Received: March 17, 2009

A novel process, i.e., ultrasound-assisted membrane reduction, was introduced and applied to synthesize Ag and Au nanocrystals. High-resolution transmission electronic microscopy and UV−vis spectra were adopted to observe and study the resulting colloids. The nearly spherical Ag and Au nanoparticles with mean diameters of 5.8 and 6.8 nm, respectively, were synthesized with the novel method. The silver nitrates/hydrogen tetrachloroaurate hydrate, sodium borohydride, and poly(*N*-vinyl-2-pyrrolidone) (PVP) were used as metal precursor, reductant, and stabilizer, respectively. The reverse mixing of silver nitrate and reductant resulted in larger Ag nanoparticles in the range of 5−24 nm. The addition of ethylenediaminetetraacetic acid (EDTA), which may serve as the second protecting agent together with PVP, could reduce the Au particle size to a mean value of 2.6 nm. By varying the $NaBH_4$ injection rate in the process, a portion of the primary Au crystallites could be self-assembled to form decahedral Au nanocrystals with a diameter of ca. 24 nm. The two-dimensional networked gold nanowires with mean diameters of 5−10 nm could be fabricated by regulating the acidity of the reaction system to pH 10 with aqueous ammonia.

1. Introduction

The gold and silver nanocrystals play important roles in different areas such as catalysis (CO oxidation),[1] chemical analysis (chemical and biological sensors),[2,3] and materials (dyes and conductive coatings).[4,5] Up to now, a number of procedures including physical and chemical methods for the synthesis of metal nanocrystals have been reported.[6−8] The methods used widely are wet chemistry techniques based on liquid-phase chemical reactions such as coprecipitation (reduction),[9,10] sol−gel processing, microemulsions[11−13] and hydrothermal (solvothermal) processing.[14,15] Among those methods, the citrate reduction raised by Faraday[16] and later modified by Frens,[17] as well as the Brust two-phase method,[18] are the most popular methods for synthesis of Au or Ag nanoparticles. However, Brust and citrate methods always faced the problems of low nanoparticle content in solution (<0.01M) and particle size restriction (1−4 nm). The proper selection of reducing or capping reagent may be efficient ways to overcome the shortages. Such as, Jana synthesized nearly monodisperse Au nanocrystals with the size adjustment of 1−15 nm by utilizing either tetrabutylammonium borohydride (TBAB) as reductant in the presence of fatty acids or aliphatic amines.[19] Hiramatsu et al. reported a novel method with the capability of producing metal nanoparticles in large scale to synthesize organoamine-protected gold and silver nanoparticles, in which only three reagents including gold or silver precursor salts, oleylamine, and a solvent were involved. They believed that the method was superior to that employed by Jana et al.[20] However, use of abundant complex agents or refluxing at higher temperature is still inevitable in wet chemistry processes. At the same time, the control of nanocrystal shape, like 1D nanochains or 2D networked nanowires, has attracted our interest but always suffers from the complicated process and higher cost.[21,22] The disadvantages may limit the practical large-scale production of metal nanomaterials.

Herein, an inexpensive, versatile, and simple method, namely Ultrasound-assisted Membrane Reduction (UAMR), is illustrated, which allows us to adjust the particle size or morphology very conveniently in PVP-protected silver and gold nanocrystal synthesis. The essential process of this method involves the chemical reduction of metal ions with reducing agent in aqueous solution, such as $NaBH_4$. The important modification of the present process is that the operational manner changes from the traditional kettle-type reaction to a flowing course. The flowing manner makes the nucleation and growth of nanocrystals occur in different locations. The crystal nucleus are generated in a membrane reactor and grow up in a circulate pipe. This is a benefit for eliminating the concentration gradient to the particle surface. The application of a ceramic membrane tube plays a crucial role for highly homogeneous dispersion of reductant and generation of the crystal nucleus. The hydrodynamical features, combined with appropriate adjustment of reaction condition, provide a favorable means to control the morphology and size distribution of metal nanocrystals. At the same time, the flowing process could improve mass transfer and reduce dead space for large-scale preparation of nanoparticles. It will be demonstrated in this paper that the silver and gold nanoparticles with different sizes, the decahedral gold nanocrystals and two-dimensional networked gold nanowires, can be synthesized by adjusting the mixing process or adding the appropriate agent to metal precursor solution in the experiment.

2. Experimental Section

The schematic diagram of the new method is presented in Figure 1. In a typical synthesis, the calculated quantities of metal precursor salts (tetrachloroauric acid or silver nitrate) and PVP as being a stabilizer were added to deionized water to form an

* To whom correspondence should be addressed. Phone: +86-10-67396588. Fax: (8610) 67396588. E-mail: hehong@bjut.edu.cn.

10.1021/jp810668x CCC: $40.75
Published on Web 04/29/2009

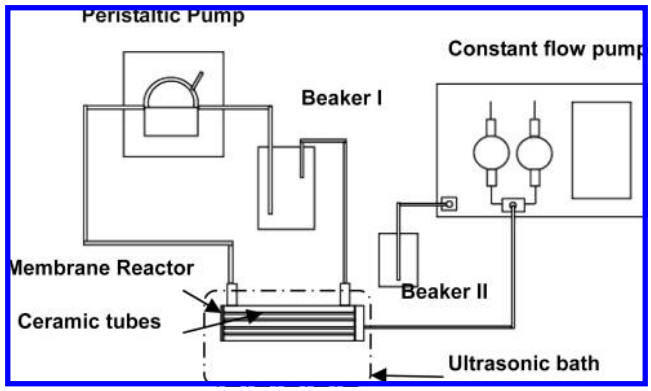

Figure 1. Schematic of ultrasound-assisted membrane reduction (UAMR) device for the synthesis of metal nanocrystals.

aqueous solution (Beaker I) under vigorous stirring. The metal precursor solution was driven by a peristaltic pump to form a cycling flow. A reductant solution (Beaker II) prepared by dissolving the desired amount of $NaBH_4$ in deionized water was injected to the membrane reactor by a constant flow pump. The reactor was composed of three ceramic membrane tubes with a canular glass tube outside. The metal precursor solution flowed in the glass tube reactor and outside the ceramic tubes. The $NaBH_4$ solution was forced into the ceramic tubes and infiltrated through the abundant holes ($\bar{d} \approx 40$ nm) on the wall of the ceramic tubes into the glass tube reactor, where the reduction of metal ions by $NaBH_4$ occurred immediately when the two solutions met. The synthesis process was stopped after complete consumption of the $NaBH_4$ solution. The membrane reactor was usually placed in an ultrasonic bath to strengthen the dispersion and mass transfer of the reactants involved in the reaction.

2.1. Synthesis of Ag Nanoparticles. $AgNO_3$(0.1 mmol) and PVP (0.6 g) were dissolved in 200 mL of deionized water to give an Ag precursor solution. The 50 mL of 0.03 mol/L $NaBH_4$ aqueous solution was used as reductant. The synthetic process was carried out according to the description above. The circulating rate of the mixture of $AgNO_3$ and PVP and the injection rate of $NaBH_4$ solution were 600 and 7 mL/min, respectively. The membrane reactor was immerged in an ultrasonic tank with a frequency of 24 kHz at room temperature. The resulted Ag colloid denoted as sample A1 was tan and ripened for 2 h. The Ag colloid (sample A2) was fabricated in the following way: The $AgNO_3$ solution was injected via the constant flowing pump into the mixture of $NaBH_4$ and PVP. The reduction and nucleation for Ag nanoparticle generation was carried out without any changes in other synthesis conditions. The Ag colloid sample from the later method was designated as sample A2.

2.2. Synthesis of Au Nanocrystals. $HAuCl_4$ (0.05 mmol) and PVP (0.6 g) were dissolved in 100 mL of deionized water to give an Au precursor solution. The 25 mL of 0.03 mol/L $NaBH_4$ aqueous solution was used as the reductant. The synthetic procedure was similar to the fabrication method of the Ag sample (A1) except that the $NaBH_4$ injection rate of 1 mL/min was adopted for the preparation of the first Au sample (A3). In the case of fabricating the second Au sample (A4), the $NaBH_4$ injection rate of 5 mL/min was kept for 1 min and then changed to 0.2 mL/min. When the third Au sample (A5) was synthesized, a solution of aqueous ammonia was added to the $HAuCl_4$ precursor solution for regulating the acidity to pH 10 before addition of PVP capping agent into the reaction system. As for the preparation of the fourth Au colloid sample (A6), the desired amount of ethylenediaminetetraacetic acid (EDTA, 0.05 g) was added into the $HAuCl_4$ solution previously keeping the other reaction conditions unchanged from the synthesis process of the first Au colloid sample (A3). The detailed synthesis conditions for samples A1−A6 are summarized in Table 1.

2.3. Characterizations. The morphology and size distribution of the Ag and Au nanoparticles were characterized by HRTEM on a JEM-2010 operating at 200 kV. The metal colloid was deposited on a carbon coating copper grid under ultrasonic pretreatment for 15 min before HRTEM examination. UV−vis spectra were recorded on a Shimadzu UV-2450 spectrometer. The spectra were collected at 200−800 nm.

3. Results and Discussion

3.1. Ag Nanoparticles. High-resolution transmission electron microscopy (HRTEM) provides extensive information about the size and crystal structure of inorganic nanoparticles. The HRTEM image of sample A1 (Figure 2, left pattern) demonstrated that spherical Ag nanoparticles could be synthesized by the UAMR process in a flowing system. The particle size was in the range of 2−11 nm (Figure 2, right pattern) with a narrow distribution and a mean diameter of 5.8 nm. Surprisingly, the spherical morphology of sample A1 remained almost unchanged and no aggregation or precipitation was observed after preservation for over 10 days without light irradiation at room temperature (Figure 3, left pattern and Figure S1 in the Supporting Information). The particle size grew a bit to a mean diameter of 6.9 nm still with a narrow distribution (Figure 3, right pattern). The stability was superior to that of Ag nanoballs reported by Yonezawa and his co-workers in similar storage media.[23] The consumption of small crystal grains (<2 nm) may account for the growth of other Ag nanoparticles because the small crystal grains were not found after storage (Figure 3).

Sample A2, which was synthesized by injecting $AgNO_3$ solution into the reductant stream, presented Ag nanoparticles with larger particle size (Figure 4, left pattern). The nanoparticles exhibited a broader distribution in the range of 5−24 nm with a mean diameter of 13.5 nm (Figure 4, right pattern). The

TABLE 1: Summary of Experimental Conditions in the Synthesis of A1-A6 Samples[d]

sample	metal precursor, mmol/L × mL	$NaBH_4$, mol/L × mL	additives	v_{injec},[b] mL/min	id_{injec}[c]	PVP/M mass ratio
A1	$AgNO_3$; 0.5 × 200	0.03 × 50	N[a]	7.0	positive	56
A2	$AgNO_3$; 2.0 × 50	0.0075 × 200	N	7.0	reverse	56
A3	$HAuCl_4$; 0.5 × 100	0.03 × 25	N	1.0	positive	60
A4	$HAuCl_4$; 0.5 × 100	0.03 × 25	N	5.0→0.2	positive	60
A5	$HAuCl_4$; 0.5 × 100	0.03 × 25	NH_3 (pH 10)	1.0	positive	60
A6	$HAuCl_4$; 0.5 × 100	0.03 × 25	EDTA (0.05 g)	1.0	positive	60

[a] No additive. [b] Injection velocity (set by the constant flowing pump). [c] Injection direction: positive = $NaBH_4$ to metal precursor solution, reverse = metal precursor to $NaBH_4$ solution. [d] Constant parameters for all syntheses in the table: PVP addition = 0.6 g; the circulating velocity = 600 mL/min; BH_4^-/M (Ag, Au) = 15/1 (molar ratio); the ultrasonic frequency = 24 kHz; atmospheric temperature.

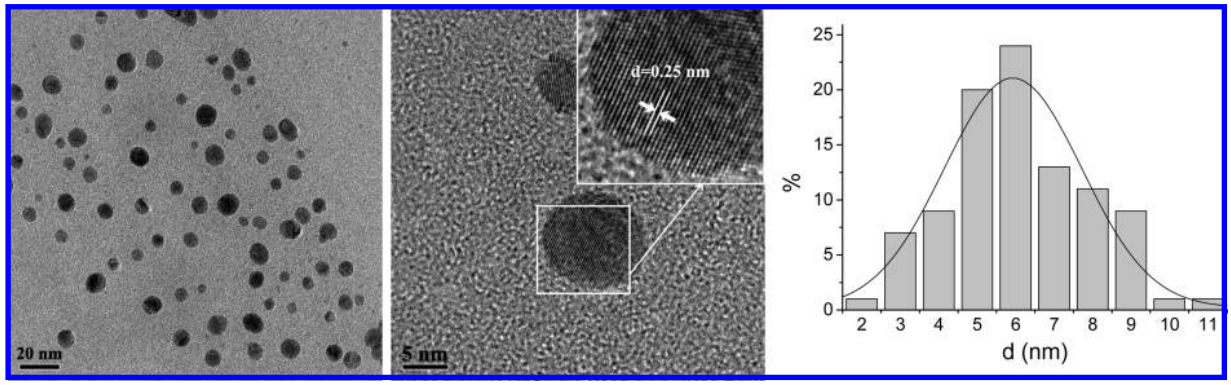

Figure 2. High-resolution TEM images (including 2-fold local magnification in the middle pattern) and size distribution of Ag nanoparticles (sample A1).

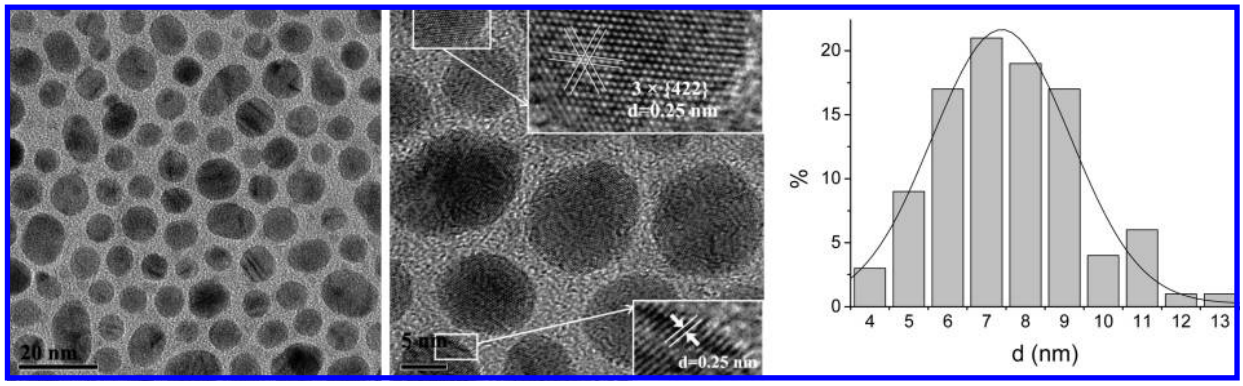

Figure 3. High-resolution TEM images (including triple local magnifications in the middle pattern) and size distribution of Ag nanoparticles (sample A1) after being stored for 10 days.

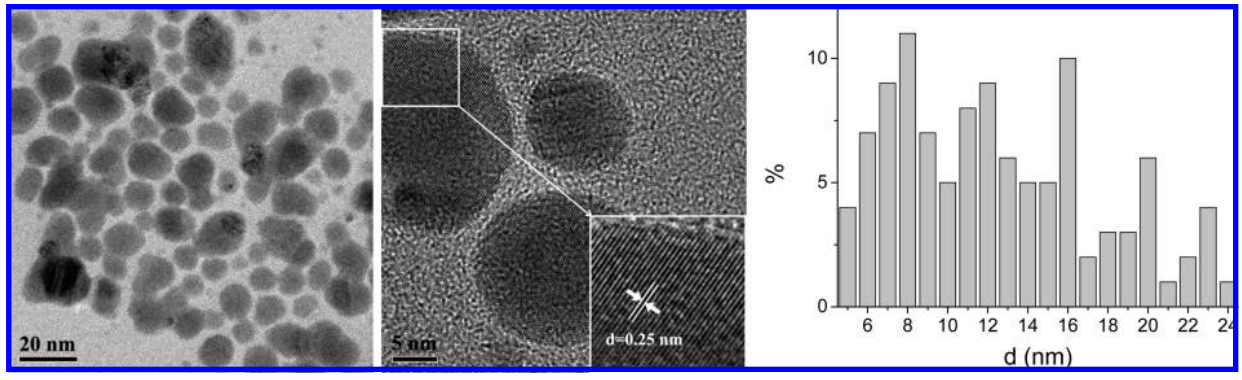

Figure 4. High-resolution TEM images (including 2-fold local magnification in the middle pattern) and size distribution of Ag nanoparticles (sample A2).

difference may be attributed to the protecting effect of PVP stabilizer. In the synthesis of sample A1, $AgNO_3$ and PVP were premixed homogeneously and the hybrid between Ag ions and capping ligands of PVP might occur. When $NaBH_4$ was injected into the tubal reactor, the reduction of Ag^+ occurred immediately to give Ag nucleus with the convenience protection, resulting in restriction of the growth of crystal nucleus. However, in the case of the synthesis of sample A2, PVP was solved into $NaBH_4$ solution as circulating flows and there was no PVP in $AgNO_3$ solution at the beginning of the sample A2 synthesis process. When $AgNO_3$ solution was injected into the mixture of PVP and $NaBH_4$ to generate the Ag nucleus, the O-donor capping ligands of PVP could not efficiently graft to the nuclear surface, leading to the growth or aggregation of Ag nanocrystals.

The middle patterns in Figures 2−4 were the corresponding magnification HRTEM images. All of them showed clear lattice fringes or a perfect lattice with 6-fold symmetry. However, the unusual periodicity, a lattice spacing of 0.25 nm, was revealed by the HRTEM. It did not match the (111) plane (0.2355 nm) of face centered cubic (fcc) crystal bulk Ag.[24] According to the literature,[25] this periodicity has been attributed to 3×(422) lattice fringes associated with 1/3(422) forbidden reflections. Many authors[26,27] observed the presence of the 1/3(422) reflections in the (111) electron diffraction pattern for Ag platelike crystals, which should be forbidden for perfect fcc structure. It was the first time this specific phenomenon for Ag nanoparticles was observed. A number of explanations for the occurrence of such kinematically forbidden reflections have been previously suggested,[25−29] which included different factors, such as the presence of atomically flat surfaces, fractionary unit cells, surface reconstructions, twin planes, and stacking faults parallel to the flat facets associated with dynamical effects of electron diffraction.

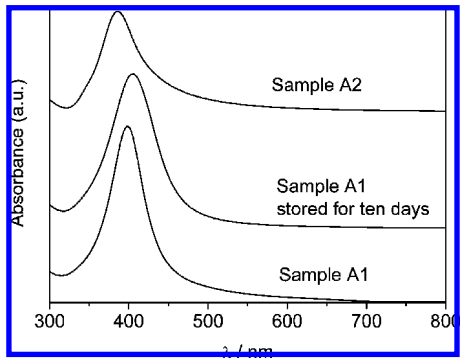

Figure 5. UV−visible absorption spectra of Ag nanoparticles.

The UV−vis absorption spectra of Ag nanoparticles were recorded and shown in Figure 5. The spectrum of the fresh Ag nanoparticle colloid (sample A1) had a surface plasmon absorption at 398 nm that was characteristic of nanocrystalline Ag nanoparticles and confirmed the low degree of their polydispersity.[30] After being stored for 10 days at room temperature, the surface plasmon adsorption peaks shifted gradually from 398 nm on the fresh sample to 405 nm, indicating the size of the Ag nanoparticles was enlarged.[31] The detailed evolution of the adsorption peak with stored time, including a two-order polynomial fitting curve, can be found in Figure S2 in the Supporting Information. The HRTEM observations of fresh and stored Ag nanoparticle samples (Figures 2 and 3) were in agreement with the data of UV−visible absorption spectra of the Ag nanoparticles and also proved the statement given by Sharma.[31] It has been known that the frequency and the strength of the resonance were determined by the size and shape of the particles as well as the dielectric function of the surrounding medium.[32,33] The decrease in particle size led to increased quantization of surface plasmon oscillation, resulting in a blue-shift of the plasmon band.[34] The absorption band centered at 386 nm with a low intensity was observed for Ag nanoparticles of A2. It was not in accordance with the enlargement in particle size, which would generally result in a red-shift. One quite possible reason was that the aggregation of small corpuscles caused the Ag nanoparticles (sample A2) to show false large particle images on HRTEM observation. However, it was understandable that the PVP stabilizers provided insufficient isolation of small Ag corpuscles in the reverse process. Therefore the Ag nanoparticles of sample A2 appearing in larger size on HRTEM images had relatively high quantization of surface plasmon oscillation and the UV−visible absorption band appeared at a lower wavelength.

3.2. Au Nanocrystals. The HRTEM and enlarged images of PVP-stabilized Au nanoparticles (sample A3) synthesized by the UAMR method were presented in Figure 6. The Au nanoparticles of sample A3 exhibited nearly spherical particles with a diameter range from 1 to 12 nm. The average diameter calculated was 6.8 nm. The clear lattice fringes with spacing of 0.235 nm validated the crystal structure of Au nanoparticles and a multiplane could also be identified (Figure 6, inset in the middle pattern). Generally, multifacets with low indices of the crystallographic plane would be presented for the fcc structure of metal nanoparticles with the lower surface energy.[35]

Nucleation, growth, ostwald ripening, and nanoparticle stabilization were general steps in the synthesis process of nanoparticles by coprecipitation (reduction). The nucleation and growth of metal nanocrytals governed the particle size and morphology of the nanoparticles in precipitation reactions. When precipitation begins, numerous small crystallites initially are generated (nucleation), but they tend to quickly aggregate together to form larger and more thermodynamically stable particles (growth).[6] The kinetic control of the nucleation and growth process may be an operative means to regulate the morphology of nanocrystals. By changing the $NaBH_4$ injection rate from 5 mL/min to 0.2 mL/min for completion in our synthesis, a portion of the small Au crystallites were self-assembled to decahedral multiply twinned particles (MTP) that were an almost perfect pentagonal bipyramid (Figure 7, left pattern) with a diameter of ca. 24 nm, which was much smaller than that of the decahedral Ag MTP reported by Marks and Howie.[36] The modeling of this structure could be deemed as the arrangements of a twin-related tetrahedral packed along (111) faces and five such units could be arranged to a decahedron. The fundamental reason for the formation of decahedral Au nanoparticles was that they contained more low-energy facets, in particular more (111) facets,[37] with the lowest system energy. It is well-known that the included angle between two faces of a regular tetrahedron was ca. 70.5°. Five tetrahedrons provided a round angle of 352.6° that left slit gaps of 7.4°. The crystal deformation should occur[35] and it was demonstrated by the distorted edge in Figure 7. The initial abundant addition of reductant resulted in fast nucleation of Au ions. Portions of Au crystallites were self-assembled into MTP in the next growth process under slow reduction. It is noteworthy that not all Au nanocrystals formed decahedral particles. To improve the yield and adjust the diameter of decahedral Au MTPs required further investigation.

Recently, organization of nanoparticles into nanowires with a networked structure has been actively studied owing to the potential uses in microelectronics, optoelectronics, nanoscale electronic devices, and other fields. In our studies, the two-dimensional networked gold nanowires could be synthesized by the UAMR method with addition of liquid ammonia (Figure 7, middle pattern of sample A5). The general view was very similar to the results reported by Pei with insufficient citrate reduction of $AuCl_4^-$.[38] The 2-D network extended to a surface area of several square micrometers and the mean diameter of nanowires was in the range of 5−10 nm as shown in the high-resolution TEM image (Figure 7). The lattice fringes were also observed corresponding to the Au (111) plane with *d*-spacing of 0.235 nm in the magnification image (Figure 7, right pattern). The ammonium ions produced a strong complexing effect with Au^{3+} (demonstrated by the disappearance of the Au^{3+} UV−vis band at 293 nm in Figure S3 in the Supporting Information), which weakened the affinity of the PVP stabilizer to the Au nanoparticles surface[18] and facilitated the adsorption of $AuCl_4^-$ while the capping agent was displaced. Thus, the force of interaction between smaller primary nanoparticles changed from a repulsive force to an attractive one under increasing van der Waals attraction.[39] This would substantially facilitate the random hit and stick of gold nanoparticles toward fusion into 1-D nanowires, which subsequently form a wirelike network structure. The coherent mechanism elucidated in detail could refer to the description by Pei et al.[38]

The introduction of additional complexing agent into the reaction solution at the initial step would affect the precipitation reaction equilibrium and the rates of crystal nucleation and growth.[6] The effect of EDTA (ethylenediaminetetraacetic acid) on the synthesis of PVP-stabilized Au nanoparticles was examined and it was found that the smaller Au nanoparticles were formed with a mean diameter of 2.6 nm with narrow size distribution (Figure 8). The inset image in the middle pattern of Figure 8 validated the single-crystal Au nanoparticle with

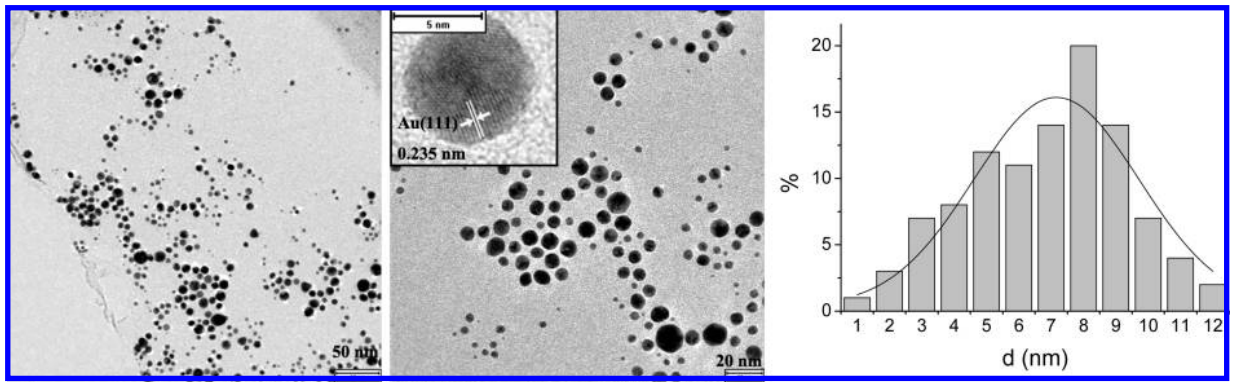

Figure 6. High-resolution TEM images and size distribution of Au nanoparticles (sample A3).

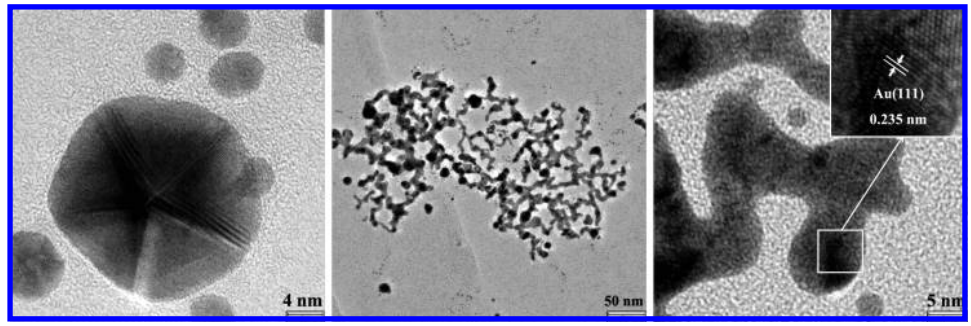

Figure 7. High-resolution TEM images of Au nanocrystals (left pattern for sample A4, middle pattern for sample A5, and right pattern for sample A5 in the magnification including triple local magnification).

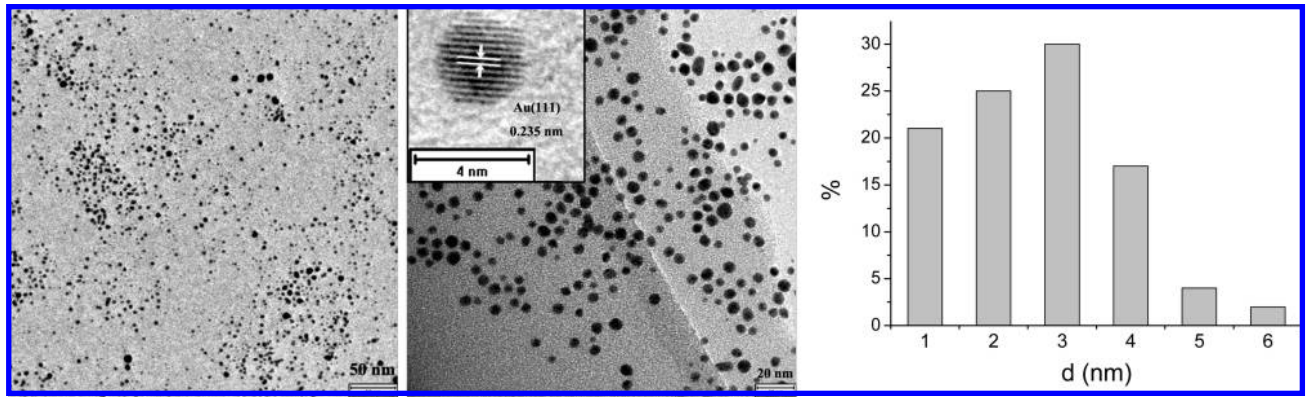

Figure 8. High-resolution TEM images and size distribution of Au nanoparticles (sample A6).

clear lattice fringes of 0.235 nm *d*-spacing corresponding to the Au (111) crystal plane. The complexing effect of EDTA to Au^{3+} was also observed from Figures S3 and S4 in the Supporting Information. The EDTA played the roles of complexing agent for ions and capping agent for charged particles through 2-N and 4-O donors. It was essential for controlling particle size in the formation of Au crystallites. The monitoring of the self-assembly process by UV−vis spectra was performed for samples A3 and A6 and the spectra were presented in Figure S4 in the Supporting Information. The low intensity of the SPR band all along was accompanied by the Au nanoparticles assembly for sample A6. Therefore, the capping effect of EDTA to Au nanoparticles immediately substituted for the complexing effect of EDTA to Au^{3+} ions as the Au^{3+} ions were reduced into Au nanoparticles, which made the EDTA the second capping agent to prevent the Au nanoparticles from growing and agglomerating.[40]

The UV−vis spectra of spherical Au (samples A3 and A6) showed that the plasmon resonance bands of gold nanoparticles were centered at ca. 535 and 520 nm, respectively, corresponding well to the calculated results from Haiss.[41] The Au decahedral multiply twinned particles (sample A4) presented a plasmon resonance band at ca. 542 nm, which should be influenced by the coexistence of smaller Au nanoparticles (d = 2−6 nm, Figure 7). The network Au nanowires (sample A5) show a flat absorption pattern with a board peak observed from 500 to 800 nm. The broad spectrum might be understood by the superposition of the longitudinal resonance of gold nanorods with various aspect ratios at relevant wavelengths. The finding was also observed for a network structure by other researchers.[38,42] The digital photographs of four colloidal Au samples is given in Figure S5 in the Supporting Information for comparison of their different colors.

It was demonstrated from the above results that well-defined Ag and Au nanoparticles could be successfully fabricated through a novel ultrasound-assisted membrane reduction method. By applying various techniques in the synthesis process, the particle size and morphology (decahedral Au nanocrystals and networked Au nanowires) could be adjusted conveniently. As we believed, most techniques were based on the adjustment of the affinity between the primary nucleus/particles surface and

the donor ligands of capping agents added into the novel membrane reduction and flowing process. In-depth research on the synthesis of colloidal Ag and Au nanocrystals based on the above preliminary results, including the formation mechanism, is in progress.

4. Conclusions

The nearly spherical silver Ag and Au nanoparticles with mean diameters of 5.8 and 6.8 nm, respectively, could be synthesized by using a novel ultrasound-assisted membrane reduction method. The fresh Ag nanoparticles grew bigger until an average size of 6.9 nm after being stored for 10 days at room temperature. The reverse mixing of silver nitrates and reductant resulted in larger Ag nanoparticles with a mean diameter of 13.5 nm. The preaddition of EDTA to gold precursor solution produced Au nanoparticles that were mostly smaller than 5 nm in particle size. The change of $NaBH_4$ injection rate from 5 to 0.2 mL/min in the synthesis process could provide the self-assembly of perfect decahedral Au nanocrystals. The two-dimensional network gold nanowires with mean diameters of 5−10 nm were assembled by regulating the acidity of the reaction system to pH 10 with aqueous ammonia.

Acknowledgment. The authors are grateful for the financial support of the National 863 Program Foundation of China (granting No. 2006AA06Z347) and the projects (granting Nos. 20877006 and 20833011) supported by the National Natural Science Foundation of China.

Supporting Information Available: High-resolution TEM images of Ag nanoparticles (sample A1) after being stored for 10 day with different magification (Figure S1), evoution of a specific UV−vis spectra peak with stored time for Ag nanoparticles (sample A1) (Figure S2), UV−vis spectra of various Au precursor solutions and Au colloidal nanocrystals (Figure S3), UV−vis spectra monitoring in the synthesis of samples A3 and A6 (Figure S4), and digial photos of four colloidal Au nanocrystals (Figure S5). This material is available free of charge via the Internet at http://pubs.acs.org.

References and Notes

(1) Comotti, M.; Li, W.-C.; Spliethoff, B.; Schüth, F. *J. Am. Chem. Soc.* **2006**, *128*, 917.
(2) Krasteva, N.; Besnard, I.; Guse, B.; Bauer, R. E.; Mullen, K.; Yasuda, A.; Vossmeyer, T. *Nano Lett.* **2002**, *2*, 551.
(3) Mirkin, C. A. *Inorg. Chem.* **2000**, *39*, 2258.
(4) Musick, M. D.; Keating, C. D.; Lyon, L. A.; Botsko, S. L.; Pena, D. J.; Holliway, W. D.; McEvoy, T. M.; Richardson, J. N.; Natan, M. J. *Chem. Mater.* **2000**, *12*, 2869.
(5) Guo, R.; Zhang, L.; Zhu, Z.; Jiang, X. *Langmuir* **2008**, *24*, 3459.
(6) Cushing, B. L.; Kolesnichenko, V. L.; O'Conno, C. J. *Chem. Rev.* **2004**, *104*, 3893.
(7) Daniel, M.-C.; Astruc, D. *Chem. Rev.* **2004**, *104*, 293.
(8) Shan, J.; Tenhu, H. *Chem. Commun.* **2007**, 4580.
(9) Yonezawa, T.; Onoue, S.; Kimizuka, N. *Langmuir* **2000**, *16*, 5218.
(10) Sharma, V. K.; Yngard, R. A.; Lin, Y. *Adv. Colloid Interface Sci.* **2009**, *145*, 83.
(11) Barnickel, P.; Wokaun, A.; Sager, W.; Eicke, H.-F. *J. Colloid Interface Sci.* **1992**, *148*, 80.
(12) Lutter, S.; Koetz, J.; Tiersch, B.; Boschetti-de-Fierro, A.; Abetz, V. *Colloids Surf., A* **2008**, *329*, 169.
(13) Zimmermann, C.; Feldmann, C.; Wanner, M.; Gerthsen, D. *Small* **2007**, *3*, 1347.
(14) Cao, J. M.; Ma, X. J.; Zheng, M. B.; Liu, J. S.; Ji, H. M. *Chem. Lett.* **2005**, *34*, 730.
(15) Chang, C. C.; Wu, H. L.; Kuo, C. H.; Huang, M. H. *Chem. Mater.* **2008**, *20*, 7570.
(16) Faraday, M. *Philos. Trans. R. Soc. London* **1857**, *147*, 145.
(17) Frens, G. *Nature (London)* **1973**, *241*, 20.
(18) Brust, M.; Walker, M.; Bethell, D.; Schiffrin, D. J.; Whyman, R. *Chem. Commun.* **1994**, 801.
(19) Jana, N. R.; Peng, X. *J. Am. Chem. Soc.* **2003**, *125*, 14280.
(20) Hiramatsu, H.; Osterloh, F. E. *Chem. Mater.* **2004**, *16*, 2509.
(21) Wu, L.; Shi, C.; Tian, L.; Zhu, J. *J. Phys. Chem. C* **2008**, *112*, 319.
(22) Tsuji, M.; Matsuo, R.; Jiang, P.; Miyamae, N.; Ueyama, D.; Nishio, M.; Hikino, S.; Kumagae, H.; Kamarudin, K. S. N.; Tang, X.-L. *Cryst. Growth Des.* **2008**, *8*, 2528.
(23) Yonezawa, T.; Onoue, S.; Kimizuka, N. *Langmuir* **2000**, *16*, 5218.
(24) Kanehara, M.; Kodzuka, E.; Teranishi, T. *J. Am. Chem. Soc.* **2006**, *128*, 13084.
(25) Germain, V.; Li, J.; Ingert, D.; Wang, Z. L.; Pileni, M. P. *J. Phys. Chem. B* **2003**, *107*, 8717.
(26) Zhang, S. H.; Jiang, Z. Y.; Xie, Z. X.; Xu, X.; Huang, R. B.; Zheng, L. S. *J. Phys. Chem B* **2005**, *109*, 9416.
(27) Rocha, T. C. R.; Zanchet, D. *J. Phys. Chem. C* **2007**, *111*, 6989.
(28) Jin, R.; Cao, Y. W.; Mirkin, C. A.; Kelly, K. L.; Schatz, G. C.; Zheng, J. G. *Science* **2001**, *294*, 1901.
(29) Maillard, M.; Suzanne, G.; Pileni, M. P. *Adv. Mater.* **2002**, *14*, 1084.
(30) Mallin, M. P.; Murphy, C. J. *Nano Lett.* **2002**, *11*, 1235.
(31) Panacek, A.; Kvitek, L.; Prucek, R.; Kolar, M.; Vecerova, R.; Pizurova, N.; Sharma, V. K.; Nevecna, T.; Zboril, R. *J. Phys. Chem. B* **2006**, *110*, 16248.
(32) Noguez, C. *J. Phys. Chem. C* **2007**, *111*, 3806.
(33) Bhui, D. K.; Bar, H.; Sarkar, P.; Sahoo, G. P.; De, S. P.; Misra, A. *J. Mol. Liq.* **2008**. DOI 10.1016/j.molliq.2008.11.014.
(34) Bernard Ng, C. H.; Yang, J.; Fan, W. Y. *J. Phys. Chem. C* **2008**, *112*, 4141.
(35) Zhang, J.; Wang, Z. L.; Liu, J.; Chen, S.; Liu, G. Y. *Self-Assembled Nanostructures*; Kluwer Academic Publishers: New York, 2002.
(36) Marks, L. D.; Howie, A. *Nature (London)* **1979**, *282*, 196.
(37) Marks, L. D. *Rep. Prog. Phys.* **1994**, *57*, 603.
(38) Pei, L.; Mori, K.; Adachi, M. *Langmuir* **2004**, *20*, 7837.
(39) Biggs, S.; Mulvaney, P.; Zukoski, C. F. *J. Am. Chem. Soc.* **1994**, *116*, 9150.
(40) Li, Y.; Guo, Y.; Liu, Y. *China Particuol.* **2005**, *3*, 240.
(41) Haiss, W.; Thanh, N. T. K.; Aveyard, J.; Fernig, D. G. *Anal. Chem.* **2007**, *79*, 4215.
(42) Chen, C. D.; Yeh, Y.-T.; Wang, C. R. C. *J. Phys. Chem. Solids* **2001**, *62*, 1587.

JP810668X